Modeling of an Optical Diaphragm for Human Pulse Pressure Detection

K. HASIKIN[1], N. SOIN[2], F. IBRAHIM[1]
[1]Department of Biomedical Engineering, Faculty of Engineering
[2]Department of Electrical Engineering, Faculty of Engineering
University of Malaya
Lembah Pantai, Kuala Lumpur
MALAYSIA
khairunnisa@um.edu.my

Abstract: - This paper presents the modeling of an optical diaphragm behavior for human pulse pressure detection. In this study, the comparison between the performance of the polyimide and silicon nitride diaphragm has been presented. The effects of diaphragm radius and diaphragm thickness on static and frequency response are also investigated. The findings show that the polyimide diaphragm is more sensitive than the silicon nitride diaphragm. In addition, deflection of both diaphragms has linear relationship with the applied pressure The diaphragm radius has more effect on the deflection, sensitivity and resonance frequency as compared to the diaphragm thickness. It can be concluded that the polyimide diaphragm achieves the optimum performance in terms of the deflection, sensitivity, and resonance frequency for human pulse pressure detection. Thus, the polyimide diaphragm has been chosen as the best model in designing an optical micro-diaphragm.

Key-Words: - Optical MEMS, Deflection, Resonance Frequency, Pressure Sensitivity, Pulse Pressure, Silicon nitride, Polyimide, Biosensor

1 Introduction

The shape of the arterial pressure waveform provides a measure of the arterial stiffness [1]. The pulse pressure waveform can be used to diagnose arterial stiffness. Arterial stiffness is caused by the buildup of fatty deposits (plaque) on the inside arteries walls. Plaques will reduce the blood flow through the artery [2].

Arterial stiffness typically begins in early adolescence, and is usually found in most major arteries [3]. However, the arterial stiffness is asymptomatic and cannot be detected by most diagnostic tools. It becomes seriously symptomatic when arterial stiffness affects coronary circulation or cerebral circulation. Furthermore, the arterial stiffness can be considered the most important underlying cause of strokes, heart attack, and various heart diseases.

Commercial miniature sensors available, regardless of their invasiveness can present only a percentage of arterial occlusions. No information about the degrees of sclerosis and stiffness of the arteries can be directly gained from them [4,5]. To obtain parameters such as distension and stiffness of the arteries, the movement of the arteries walls during pulsation must be accurately detected. Several techniques have been used in recent years. This includes Magnetic Resonance Imaging (MRI), angiography, Intravascular Ultrasound (IVUS) and biomedical pressure sensor.

The MRI is an imaging technique used primarily in medical settings to produce high quality images of the inside of human body [6]. It provides detailed images of the body in any plane. MRI is potentially useful and can be used as an effective diagnostic tool in basic research, clinical investigation and disease diagnosis [7]. It provides both chemical and physiological information of the tissue in human body [7,8]

However, many magnetic resonance signals face the problem of low signal-to-noise ratio [7,9]. Due to this complication, magnetic resonance image estimation from noisy data is challenging.

The angiography technique is also used in the diagnosis of the arterial stiffness. Angiography involves looking inside the arteries to see if there is any blockage in the arteries wall [10]. This is the most accurate way to assess the presence and the severity of vascular diseases [10]. However, angiography is invasive and relatively high cost as compared to other diagnosis techniques.

The IVUS enables assessment of morphology and distribution of in vivo plaque [11]. It uses a catheter with a miniaturized ultrasound probe that can determine plaque volume within the arterial wall. The IVUS can visualize the lumen of the arteries. However, IVUS is time consuming and can only be performed by a technician who is trained in interventional cardiology techniques [10]. In addition, there may be an additional risk imposed by the use of the IVUS catheter.

The biomedical pressure sensor has shown its potential in the diagnosis of arterial stiffness. Diagnosis of arterial stiffness can be conducted by detecting the pulse pressure on the radial artery. There are two approaches in biomedical pressure measurements

namely, direct and indirect pressure measurements. The direct pressure measurement refers to the assessment of the pressure using a sensor that is in contact with blood or fluid in human body [12]. Through this invasive techniques, the sensor experiences physical connection with circulating blood or measured fluid.

However, indirect pressure measurement involves a sensor that does not utilize any invasive measurements. Advancement in semiconductor technology has revolutionized the designing biomedical pressure sensor. Nevertheless, there is critical need for a miniature ultra-low pressure transducer [13]. Many sensing principles such as piezoresistive, capacitive and optical have been looked into biomedical pressure sensing. Rapid expansion in Biological Micro-electro-mechanical Systems (BioMEMS) has enabled sensor miniaturization for arterial pressure measurements.

Sensing principles such as capacitive and piezoresistive have shown good potential in biomedical applications. However, a major problem associated with the piezoresistive pressure sensor is its inherent sensitivity to temperature [14-16].

In contrast to the piezoresistive pressure sensors, it is well known that the capacitive detection principle has a high sensitivity. However, electrical connections to the sensor are very sensitive to noise. This is due to small electrical capacitance. Therefore, electrical connections have to be made as short as possible and this makes the sensor packaging process a big challenge. [14].

Optical sensor has the advantage of high resolution, high sensitivity, intrinsic electrical passivity and immunity to electromagnetic interference [17-19]. Optical sensor typically utilizes a sensor head that consists of a diaphragm and optical fiber which in turn, converts the light rays to electric signal. The diaphragm is one of the most important parts in the optical sensor because the sensitivity of the sensor is highly dependent on its performance [13].

This paper presents the modeling of an optical micro-diaphragm for human pulse pressure detection. The effect of diaphragm material, radius and thickness on static and frequency responses are analyzed.

2　Theory of a Circular diaphragm

This section discussed the theory of circular diaphragm on deflection, sensitivity and resonance frequency of the diaphragm are presented.

2.1 Diaphragm deflection under applied pressure

Load-deflection method is used for elastic properties measurement of thin films [14, 20-22]. In this technique, the deflection of a fixed edge diaphragm is measured as

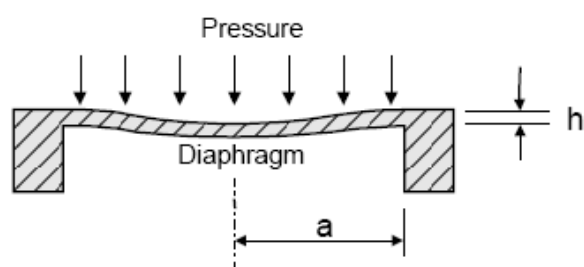a function of applied pressure as shown in Figure 1.

Figure 1: Structure model for the circular diaphragm

The diaphragm will be deflected under a uniform applied pressure. The out-of-plane deflection of the diaphragm, y is a function of the pressure difference and the radial distance [10-12]:

$$y = \frac{3(1-\mu^2)P}{16Eh^3}(a^2 - r^2)^2 \qquad (1)$$

where y is deflection, P is applied pressure, μ is Poisson's ratio, E is Young's Modulus, h is diaphragm thickness, a and r are effective diaphragm radius and radial distance, respectively.

The maximum deflection, of the diaphragm as a function of applied pressure can be written as [11]:

$$y_c = \frac{3(1-\mu^2)a^4}{16Eh^3}P \qquad (2)$$

When the diaphragm is thick, the flexural rigidity of the diaphragm will increase. Flexural rigidity is defined as a force couple required to bend a rigid structure and can be defined as:

$$D = \frac{Eh^3}{12(1-v^2)} \qquad (3)$$

The relationship between the flexural rigidity and deflection is shown as in equation (4).

$$y_c = \frac{P(a^4)}{64D} \qquad (4)$$

2.2　Pressure Sensitivity

The pressure sensitivity (Y) is defined as the ratio between the deflection and the pressure difference [5, 11]. Sensitivity is normally used in evaluating the performance of the diaphragm as it is a pressure sensitive element. When the optical fiber is positioned facing the center of the diaphragm, the maximum deflection and pressure sensitivity will be analyzed.

As for silicon nitrite and polyimide

diaphragms, their pressure sensitivity at the center of the diaphragm is given by equations (5) and (6) respectively [11]:

$$Y_c(siliconnit\ ride) = 8.585 \times 10^{-11} \frac{a^4}{h^3} (\mu m/mmHg) \quad (5)$$

$$Y_c(polyimide) = 2.194 \times 10^{-11} \frac{a^4}{h^3} (\mu m/mmHg) \quad (6)$$

where diaphragm radius (*a*) and diaphragm thickness (*h*) are in microns.

2.3 Resonance Frequency

Frequency response is another important issue in modeling of the micro-diaphragm. In this study, the diaphragm is defined as a free vibrating circular plate clamped rigidly at the edge. Resonance frequency of the diaphragm is given by [5, 11]:

$$f_{mn} = \frac{\alpha_{mn}}{4\pi} \sqrt{\frac{E}{3\rho(1-\mu^2)}} \left(\frac{h}{a^2}\right) \quad (7)$$

where α_{mn} and ρ are constants related to the vibrating modes of the diaphragm and mass density of the diaphragm material, respectively.

3 Principle of operation

The optical pulse sensor consists of an optical fiber and a micro-diaphragm structure as pressure transducer. It is demodulated by detecting the shift of the reflected or transmitted spectrum from the light source. Light emitting diode (LED) is used as a light source and the light emitted will then be transmitted via optical fibers.

Pulse pressure that is sensed from the surface of radial artery, will cause deformation of the diaphragm. This deformation will change the reflected or transmitted spectrum. The diffused components of the reflected light will strike the diaphragm which is in contact with the skin on the radial artery.

From the reflected spectrum, the cavity length of the sensor, deflection and corresponding pressure can be measured. The reflected waveform will provide the information on the arterial stiffness and elasticity of the artery [1].

However, this study focuses on the modeling of an optical micro-diaphragm for the human pulse pressure detection. The modeling and analysis of the diaphragm are presented in the next subsection. The analysis includes the static and frequency response of the diaphragm and the diaphragm material is chosen based on this analysis.
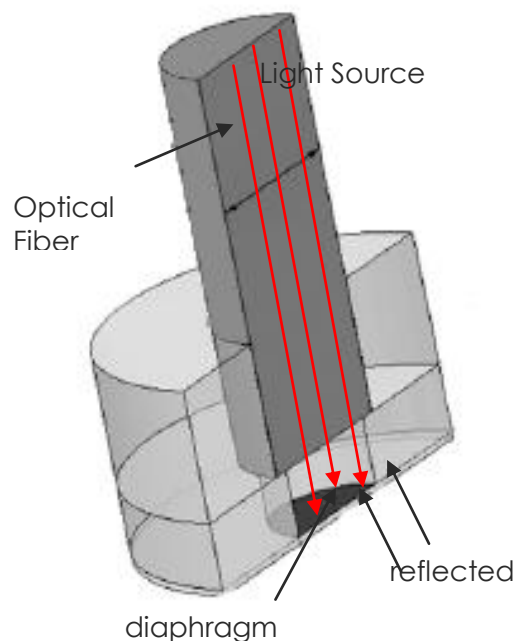

Figure 2: Proposed design of the optical MEMS sensor [4].

4 Design Specifications

The optical sensor is targeted to sense the pulse pressure on the surface of human's radial artery. According to [23-25], the diameter of normal human artery is between 2.5 to 3mm. Therefore, the overall sensor system must be smaller than the size of radial artery.

Since the sensor is externally attached to the human wrist, the pulse pressure will not create the same pressure as the blood exerts on the arteries wall [23]. The pressure will not be sufficient enough to displace the diaphragm by more than 1μm [23]. Therefore, miniature size diaphragm with maximum deflection of 1μm is needed.

In order to ensure the diaphragm operates in a linear range, the resonance frequency of the diaphragm should be at least 2.5 times larger than the applied frequency [26]. For pulse pressure detection, the diaphragm should be able to operate in the frequency range from 0 to 50 kHz. The complete diaphragm specifications are presented in Table 1.

Table 1: Diaphragm Specifications

Parameter	Value
Pressure range	0-300mmHg
Frequency range	0-50kHz
Maximum Deflection	$\leq 1\mu m$

Hence, to successfully perform pulse pressure measurement, the sensor should have the following characteristics [26]:

- biocompatibility
- adequate detection system to measure small diaphragm deformation
- miniature in size
- appropriate dynamic range and sensitivity for small pulse pressure measurement.

5 Methodology

In this research, the circular diaphragm is designed by using MEMS CAD Software, *(Intellisuite)*. The 3D model of the diaphragm was constructed using the fabrication process editor in *Intellifab* module. Due to negligence of residual stress at the edge of surface of the diaphragm, the circular shape has been chosen for the diaphragm.

Fabrication process in *Intellifab* module consists of three layers of materials. A 2μm release layer of silicon dioxide film is deposited on silicon wafer by plasma-enhanced chemical vapor deposition (PECVD) using tetraethoxysilane (TEOS). Then, a second layer is deposited on top of the release layer. This second layer is the diaphragm material which is either silicon nitride or polyimide. The second layer which is 30μm thick forms the cylindrical wall around the cavity of the sensor system.

Diameter hole and cavity wall are patterned by using deep reactive ion etching. The diameter hole is smaller than the cavity wall to act as an insertion stop for the optical fiber. To enhance reflection from the diaphragm, metal was evaporated onto the entire wafer. A layer of 200Å chromium and a layer of 1000Å titanium were then coated on the wafer respectively. After developing the diaphragm, micromanipulator will be used to insert cleaved end of a single mode optical fiber. Steps in the fabrication process are simplified in Figure 3.
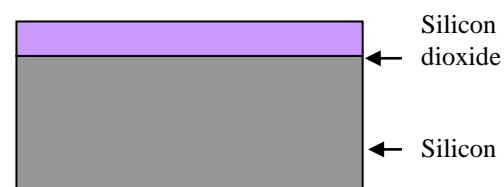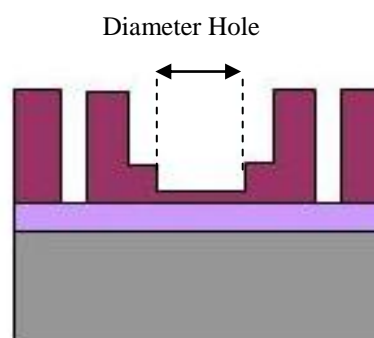

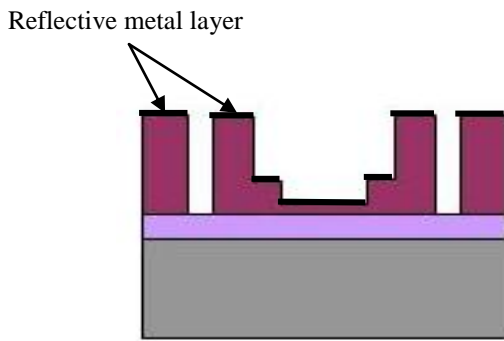(a) Release layer of silicon dioxide is deposit onto the silicon wafer
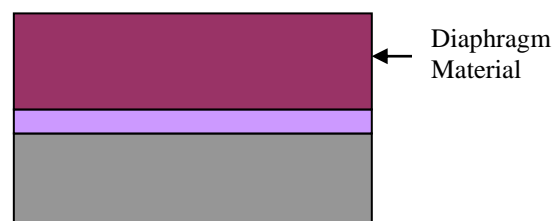
(b) Deposition of diaphragm material onto the silicon wafer
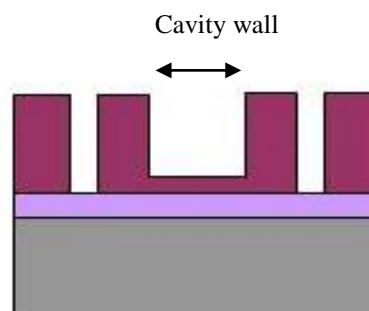
(c) Developing the cavity wall

(d) Diameter hole is formed by using DRIE

Reflective metal layer

(e) Reflective metal layer is evaporated onto the whole wafer

Figure 3: Fabrication process for the circular diaphragm. (a) Release layer (2μm silicon dioxide) is deposit onto the silicon wafer. (b) Diaphragm material is deposit onto the wafer as diaphragm layer. (c) Diameter hole is pattern by using deep reactive ion etching (DRIE). (d) Etching process using DRIE to form cavity walls. (e) 200Å chromium and 1000Å Titanium will be evaporated onto the whole wafer as a reflective metal layer.

The analysis of the diaphragm has been performed by using *Thermoelectromechanical* module once the realization of the diaphragm structure was completed. The *Thermoelectromechanical* module is a type of analysis which is based on the finite element method.

The finite element analysis (FEA) also known as finite element method is a computational technique used to obtain approximate solutions of boundary condition problems in engineering [27]. Before fabricating the diaphragm, it is essential to do a theoretical analysis by using the FEA. This analysis is helpful because FEA gives close approximation of the actual prototype before it is fabricated.

Enormous amount of time and money can be saved by using the FEA because any difficulties that may rise during designing of the diaphragm can be detected and rectified at an early stage. Hence, trial and error approaches which are in use today can be avoided [27]. In addition, the FEA is a simulation technique that can be used to analyze the behavior of MEMS devices [28].

To design the diaphragm by using FEA, it is necessary to define the type of construction elements, mesh profile, material properties, boundary conditions and loads [29-31]. The movable diaphragm in FEA simulation must operate in a small deflection region and must have a perfect boundary condition.

Boundaries of the diaphragm are fixed and clamped at its edge as shown in Figure 4. Three-dimensional model of the diaphragm in Figure 5 is meshed and discretized into elements for FEA

simulation in *Thermoelectromechanical* module. Figure 5 shows the 3D model of the diaphragm before and after meshed.
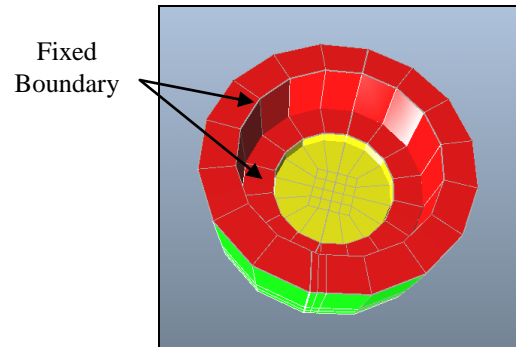
Fixed Boundary

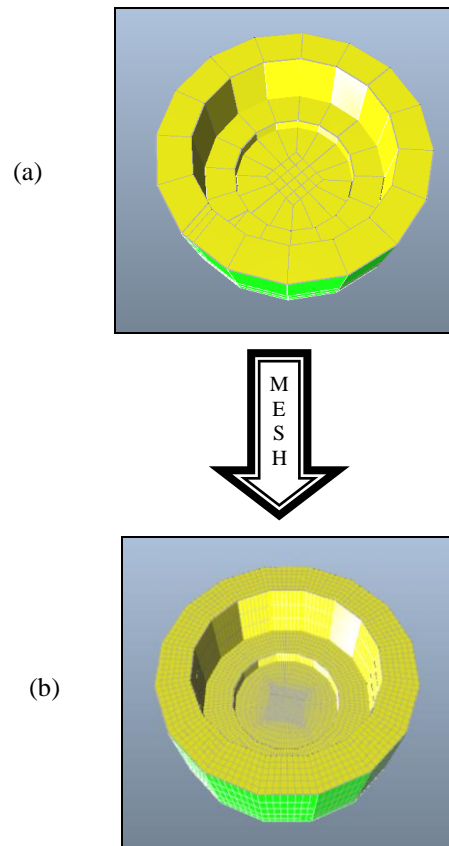Figure 4: Diaphragm with fixed boundary

(a)

M
E
S
H

(b)

Figure 5: 3D diaphragm model (a) before meshed and (b) after meshed

Two types of diaphragm materials are used to compare the performance of the diaphragm. The materials used are polyimide and silicon nitride. The comparison of material properties between silicon nitride and polyimide is shown in Table 2. Since the diaphragm is designed to detect the pulse pressure, it is loaded with the pressure range from 0 to 300mmHg as presented in Table 1[2].

The diaphragm radius and diaphragm thickness

are also varied in order to study their effects on diaphragm's behavior. The best model will be chosen.

Table 2: Material Properties of Silicon Nitride and Polyimide

Material Properties	Silicon Nitride	Polyimide
Young's Modulus (GPa)	270	7.5
Poisson Ratio	0.27	0.35
Thermal Conductivity (W/cm/C)	0.032	8.06×10^{-6}
Specific Heat (J/gC)	0.71	4.21
Electrical Resistivity (Ωcm)	0.6	1×10^{-16}
Dielectric Constant	7.5	3.4
Density (g/cm^3)	3.44	1.33
Coefficient of Thermal Expansion (/°C)	2810×10^{-7}	810×10^{-7}

6   Results & Discussions

The simulation results are shown in Figures 6 to 12. Figure 6 illustrates the deflection in relation with diaphragm radius and diaphragm thickness. The 3-dimension graphs for the diaphragm's sensitivity and resonance frequency are illustrated in Figures 7 and 8, respectively.

At a particular diaphragm thickness, the deflection and sensitivity increase as diaphragm radius increases (Figures 6 and 7). The result also indicates that the thinner the diaphragm thickness, the higher the deflection. This is phenomena is supported by Equations (1) and (2).

Figure 6: The relationship among diaphragm radius, diaphragm thickness and deflection

Figure 7: The relationship among diaphragm radius, diaphragm thickness and sensitivity

Figure 8 illustrates that the resonance frequency increased as the diaphragm radius and diaphragm thickness are small and thick respectively as supported by equation (7). The results indicate that the diaphragm radius has more effect on deflection, sensitivity and resonance frequency as shown in Figures 6 to 8.
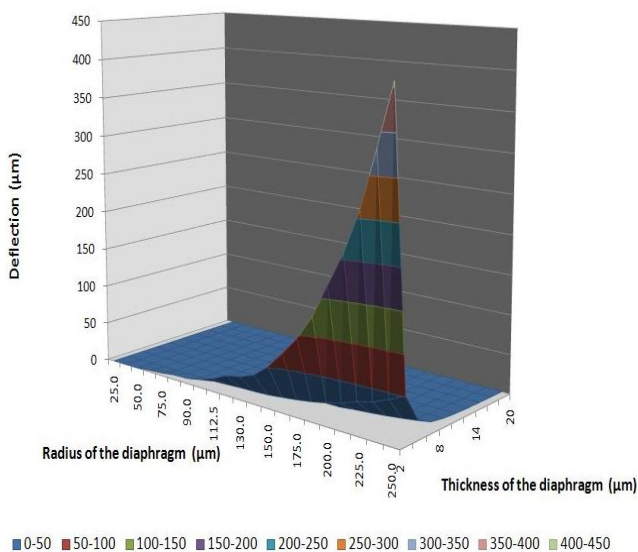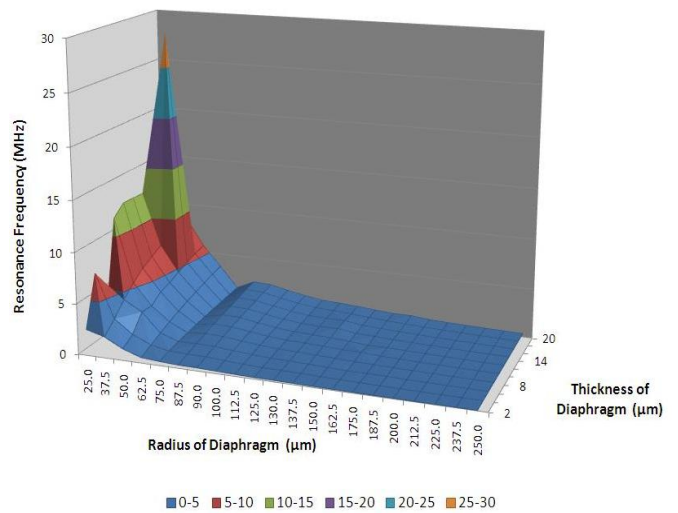

Figure 8: The relationship among diaphragm radius, diaphragm thickness and resonance frequency

The deflection curve for polyimide and silicon nitride diaphragms under applied pressure are shown in Figure 9. From this figure, it can be observed that the deflection increased from outer surface to the center of the diaphragm. Thus, the maximum deflection occurs when the radial distance, is at the center of the diaphragm($r=0$). The maximum deflections of

polyimide and silicon nitride diaphragms are 0.9μm and 0.02μm respectively (Figure 9).

Figure 10 depicts the sensitivity versus the radius of silicon and polyimide diaphragms. Both diaphragms show an increase of sensitivity as the diaphragm radius increases. However, the results show that the polyimide diaphragm is more sensitive. This finding is supported by the other researchers [14, 20, 22, 25, 32, 33]. The silicon nitride diaphragm possesses higher Young's Modulus and stiffer than the polyimide diaphragm (Table 2). Thus, the silicon nitride diaphragm is less sensitive than the polyimide diaphragm. Based on the findings shown in Figures 9 and 10, it can be concluded that the polyimide diaphragm achieves a higher deflection and more sensitive than silicon nitride diaphragm.
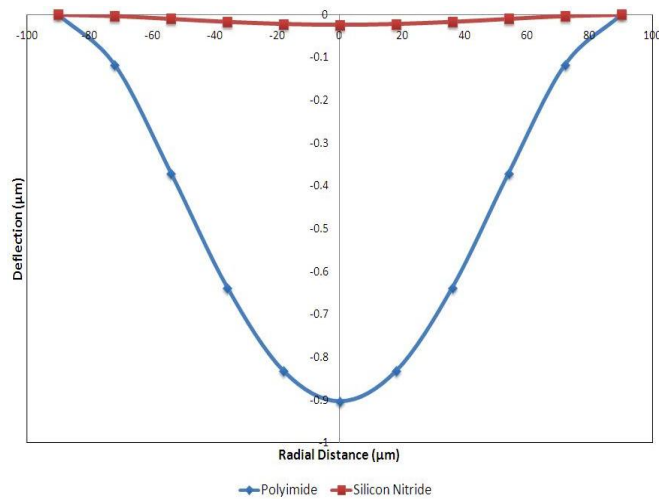

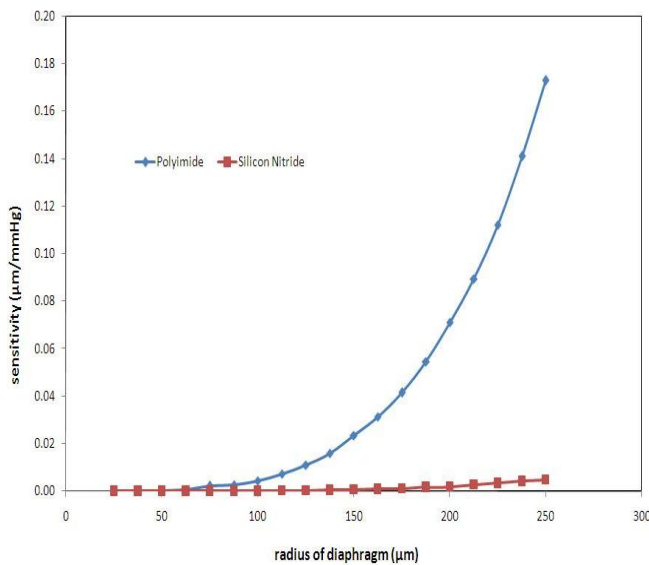Figure 9: Deflection curve under applied pressure.

Figure 10: Comparison of sensitivity between polyimide and silicon nitride diaphragms

The comparison of resonance frequency between silicon nitride and polyimide diaphragm is shown in Figure 11. In contrast with the deflection and sensitivity, resonance frequency decreases when diaphragm radius is large. This behavior can also be supported by equation (7). It can be concluded that the resonance frequency of polyimide diaphragm is lower than silicon nitride diaphragm. Although the given resonance frequency is low, the polyimide diaphragm has higher deflection and more sensitive than silicon nitride diaphragm.

Equation (2) indicates that the maximum deflection is proportional to the applied pressure. In addition, linear deflection-pressure relationship is highly desirable in designing the diaphragm [21, 22]. This is because with such a linear relationship, the behavior of the diaphragm is easier to calculate and measured [21,22].
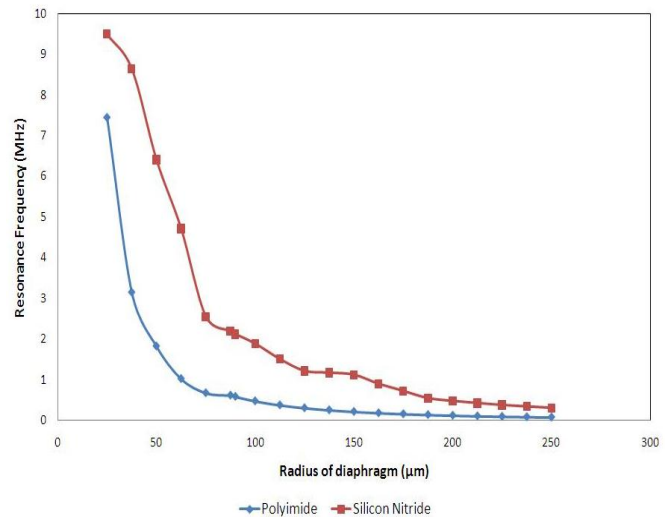

Figure 11: Comparison of resonance frequency between polyimide and silicon nitride diaphragms

Figure 12 shows the deflection increases linearly when both diaphragms are loaded with the pressure. The result illustrates that the polyimide diaphragm has higher deflection as compared to the silicon nitride diaphragm. This is due to the increased of flexural rigidity in silicon nitride diaphragm. The deflection is decreased when the flexural rigidity of the diaphragm is increased as supported by equations (3) and (4) [21].

Simulation results in Figures 9 to 12 have shown that the polyimide diaphragm achieves optimum performance in sensing the human pulse pressure as compared to silicon nitride diaphragm. The maximum deflection and resonance frequency of polyimide diaphragm are 0.9μm and 0.58MHz, respectively. The sensitivity for polyimide is 0.003μm/mmHg.
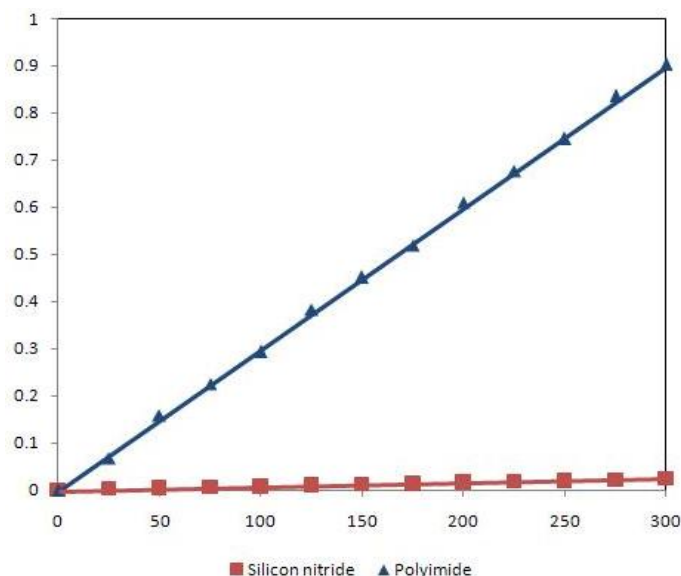
Figure 12: The deflection-pressure relationship for polyimide and silicon nitride diaphragms.

7 Conclusion

The modeling of an optical micro-diaphragm for human pulse pressure detection has been presented. The simulation results for both diaphragms showed that when the diaphragm radius and diaphragm thickness are large and thin respectively, the deflection and sensitivity increased whilst the resonance frequency decreased.

Diaphragm's behavior on deflection, sensitivity, and resonance frequency are supported by analytical equations in Section 2 and in agreement with other researchers' findings [5, 10, 12, 15-16]. In addition, deflection of silicon nitride and polyimide diaphragms is linearly correlated with the applied pressure.

The simulation findings indicate that polyimide diaphragm provides higher sensitivity and lower resonance frequency than silicon nitride diaphragm. Polyimide diaphragm achieved optimum performance and was proven to be the best model for designing an optical micro-diaphragm. The maximum deflection and sensitivity of polyimide are 0.9 μm and 0.003μm/mmHg, respectively. The resonance frequency of the polyimide diaphragm is 2.5 times larger than the applied frequency. Therefore, the polyimide diaphragm operated in optimum frequency response and satisfied the maximum allowable deflection.

Acknowledgment

References:

1. Wilkinson, I.B., Hall, I.R., MacCallum, H., Mackenzie, I.S., McEniery, C.M., Van der Arend, B.J., Yae-Eun, S., Mackay, L.S., Webb, D.J., Cockcroft, J.R., Pulse Wave Analysis Clinical Evaluation of a Noninvasive, Widely Apllicable Method for Assessing Endothelial Function. *Arterioscler Thromb Vasc Biol*., Vol. 22, 2002, pp. 147-152.

2. Latifoglu, F., Sahan, S., Kara, S., Gunes, S., Diagnosis of atherosclerosis from carotid artery Doppler signal as a real world medical application of artificial immune systems. *Expert Systems with Applications.* Vol. 33, 2007, pp. 786-793.

3. Alty, S.R., James, N.A., Millasseau, S.C., Chowienczyk, P.J., 2007. Predicting Arterial Stiffness from Digital Volume Pulse Waveform. *IEEE Transaction on Biomedical Engineering*, 54(12), pp. 2268-2275.

4. Pouladian, M., Golpayegani, M.R.H., Noninvasive detection of a atherosclerosis by Arterio-Oscillo-Gram. *Proceedings of the 25th Annual International Conference of the IEEE EMBS*. September 17-21, 2003.

5. Hill, G.C., Melamud, R., Declercq, F.E., Davenport, A.A., Chan, I.H., Hartwell, P.G. SU-8 MEMS Fabry-Perot Pressure Sensor. *Sensors and Actuators A Physical*, 2007, Vol. 138, No. 1, pp. 52-62.

6. Hossain, M.I., Abedin, A.H., 2008. Magnetic resonance angiography – an advanced technique in MRI using flow imaging. In: LISSA 2007, *IEEE/NIH Life Science Systems and Applications Workshop*, 2007. LISA 2007. Nov 8-9, 2007.

7. Yu, H, Zhao, L., 2008. An efficient denoising procedure for magnetic resonance imaging. In: ICBBE 2008, *The 2nd International Conference on Bioinformatics and Biomedical Engineering*. Shanghai, China. 16-18 May, 2008.

8. Hautvast, G., Lobregt, S., Breeuwer, M., Gerritsen, F., 2006. Automatic contour propagation in cine cardiac magnetic resonance images. *IEEE Transaction on Medical Imaging*. 25 (11), pp. 1472-1482.

9. Gravel, P., Beaudoin, G., De Guise, J. A., 2004. A method for modeling noise in medical images, *IEEE Trans. Med. Imag.*, 23 (10), pp. 1221-1232.

10. Andreoli, T.E., Bennett, J.C., Carpenter, C.J., Plum, F., 2001. *Cecil Essentials of Medicine*,

50th Edition, Philadelphia, Pennsylvania: Saunders.

11. Yamagishi, M., Terashima, M., Awano, K., Kijima, M., Nakatani, S., Daikoku, S., Ito, K., Yasumura, Y., Miyatake, K., 1999. Morphology of Vulnerable Coronary Plaque: Insights from Follow-up of Patients Examined by Intravascular Ultrasound before an Acute Coronary Syndrome. *Journal of American College of Cardiology*, 35(1), pp.106-111.

12. Dorf, R.C., 2006. *Sensors, Nanoscience, Biomedical Engineering, and Instruments*. 3rd Ed. CRC Press.

13. Noh, H-S, Kim, S., Hesketh, P.J., Mao, H., Wong, L. 2003. Miniature Corrugated Diaphragm for Fiber-Optic-Linked Pressure Sensing (FOLPS). IN IMECE '03, 2003 ASME International Mechanical Engineering Congress & Exposition, Washinton, D.C., USA, 16-21 November 2003.

14. Xu, J., *High Temperature High Bandwidth Fiber Optic Pressure Sensors*. Ph.D. Blacksburg, Virginia: Virginia Polytechnic and State University. 2005.

15. Kerr, D.R., Milnes, A.G.,. Piezoresistance of Diffused Layers in Cubic Semiconductors. *Journal of Applied Physics*, 34, 1963, pp. 727-731.

16. He, R., & Yang, P., Giant Piezoresistance Effect in Silicon Nanowires. *Nature Nanotechnology*, 1, 2006, pp. 42-46.

17. Totsu, K., Haga, Y., Esashi, M., 2005. Ultra-Miniature Fiber-Optic Pressure Sensor using White Light Interferometry. *Journal of Micromechanics and Microengineering*, 15, pp. 71-75.

18. Tohyama, O., Kohashi, M., Sugihara, M., Itoh, H., 1998. A Fiber-Optic Pressure Microsensor for Biomedical Applications. *Sensors and Actuators A*, 66, pp. 150-154.

19. Toshima, K., Watanabe, T., Kaneko, Y., Maesako, T., Takakashi, K., Diaphragm-Type Optical Fiber Pressure Sensor with a Sleeve Fiber Insertion. In MHS 2003, *International Symposium on Micromechatronics and Human Science*. Nagoya Municipal Industrial Research Institute, 19-22 October 2003.

20. Eaton, W.P., Bitsie, F., Smith, J.H., Plummer, D.W. A New Analytical Solution for Diaphragm Deflection and Its Application to a Surface-Micromachined Pressure Sensor, *International Conference on Modeling and Simulation of Microsystem*.

21. Giovanni, M.D. Flat and Corrugated Diaphragm Design Handbook Marcel Dekker, Inc. 1982.

22. Soin, N., Majlis, B.Y. An Analytical Study on Diaphragm Behavior for Micro-machined Capacitive Pressure Sensor. *International Conference on Semiconductor Electronics*, 2002.

23. Le, H.P., Shah, K., Singh, J., Zayegh. A. Design and Implementation of an Optimised Wireless Pressure Sensor for Biomedical Application *Analog Interg Circ. Sig. Process*, Vol. 48., 2006, pp. 21-31.

24. Madssen, E., Haere, P., Wiseth, R. Radial Artery Diameter and Vasodilatory properties After Transradial Coronary Angiography. *Ann Thorac Surg.*, Vol. 82., 2006, pp.1698-1703.

25. Osika, W., Dangardt, Gronros, F.J., Lundstam. U., Myredal, A., Johansson, M., Volkmann, R., Gustavsson, T.,Gan, L. M., Friberg, P. Increasing Peripheral Artery Intima Thickness from Childhood to Seniority. *Journal of The American Heart Association*, 2007, Vol. 27, No. 3, pp. 671-676.

26. Wang, X., Li, B., Russo, O.L., Roman, H. T., Chin, K.K., Farmer, K.R., Diaphragm design guidelines and an optical pressure sensor based on MEMS technique, *Microelectronic Journal*, Vol. 37, 2006, pp. 50-56.

27. Shirazee, N.A., Basak, A., Nakata, T., Takahashi, N., 1997. Analysis of Permanent Magnet Lifting Devices using Finite Elements, *IEEE Transactions on Magnetics*, 33(2), pp. 2211-2214.

28. Goldberg, R.L., Jurgens, M.J., Mills, D.M., Henriques, C.S., Vaughan, D., Smith, S.W., 1997. Modeling of Piezoelectric Multilayer Ceramics using Finite Element Analysis. *IEEE Transactions on Ultrasonics, Ferroelectronics and Frequency Control*, 44(6), pp. 1204-1214.

29. Senturia, S.D., 2001. *Micro System Design,* Kluwer Academic Publishers.

30. Correia, J.H., Bartek, M., Wolffenbuttel, R.F., 1998. Load-deflection of a Low Stress SiN-Membrane/Si Frame Composite Diaphragm. In *Technical Proceedings of the 1998 International Conference on Modeling and Simulation of Microsystem* , Puerto Rico, USA.

31. Taylor, Z.A., Cheng, M., Ourselin, S., 2008. High-Speed Nonlinear Finite Element Analysis for Surgical Simulation Using Graphics Processing Units. *IEEE Transactions on Medical Imaging*, 27(5), pp. 650-663.

32. Sun, Y., Feng, G., Georgiou, G., Niver, E., Noe, K., Chin, K., Center Embossed Design Guidelines and Fabry-Perot Diaphragm Fiber

Optic Sensor. Microelectronic Journal, Vol. 39, 2008. pp. 711-716

33. Hasikin, K., Ibrahim, F., Soin, N. Determination of design parameters for human artery pulse wave detection, In IFMBE 4th International Conference on Biomedical Engineering, Kuala Lumpur, 25-28 June 2008.

34. Xiao-qi, N., Ming, W., Xu-xing C., Yi-xian, G and Hua R., An Optical Fiber MEMS Pressure Sensor Using Dual-Wavelength Interrogation. *Measurement science and technology*, Vol. 17, No. 9, 2006, pp 2401- 2404.